The Magnetic Anisotropy Effectiveness on NiFe$_2$O$_4$ and NiFe$_2$O$_4$@SiO$_2$ Nanoparticles for Hyperthermia Applications

Mustafa COSKUN[1]*, Senem CITOGLU[2], Mustafa KORKMAZ[1], Tezer FIRAT[1]

[1] *Department of Physics Engineering, Hacettepe University, 06800, Beytepe, Ankara / TURKEY*

[2] *Department of Nanotechnology and Nanomedicine, Hacettepe University, 06800, Beytepe, Ankara / TURKEY*

Abstract: In this study, we analyzed the magneto-heating properties of NiFe$_2$O$_4$ nanoparticles, coated with a SiO$_2$ shell for hyperthermia applications. The NiFe$_2$O$_4$ nanoparticles were synthesized and coated with SiO$_2$ by chemical route and water in oil techniques, respectively. The size of core particles is ~5.6±0.1 nm and the thicknesses of the SiO$_2$ layers around the core change from 0 nm to 14.1±0.1 nm by increasing the amount of tetraethyl orthosilicate from 0 ml to 2.5 mL during the synthesis process. The magnetic anisotropies, obtained from magnetic susceptibility measurements have the same behavior with the specific heat absorption ratio of the samples.

Keywords: Magnetic materials, nanostructures, chemical synthesis, magnetic properties.

Hipertermi Uygulamaları İçin NiFe$_2$O$_4$ ve NiFe$_2$O$_4$@SiO$_2$ Nanoparçacıklarının Manyetik Anizotropi Etkinliği

Özet: Bu çalışmada, hipertermi uygulamaları için SiO$_2$ ile kaplanmış NiFe$_2$O$_4$ nanoparçacıklarının magnetik-ısıtma özellikleri analiz edildi. NiFe$_2$O$_4$ nanoparçacıkları kimyasal yöntemle sentezlenerek, mikroemülsiyon tekniğiyle SiO$_2$ ile kaplandı. Çekirdek parçacıklarının boyutu 5.6 ± 0.1 nm'dir. Kaplama sürecinde çekirdek çevresindeki SiO$_2$ tabakasının kalınlıkları tetraetil ortosilikat miktarı 0 mL'den 2.5 mL'ye arttırılarak 0 nm'den 14.1 ± 0.1 nm'ye kadar değiştirilmiştir. Manyetik duyarlılık ölçümlerinden elde edilen manyetik anizotropi değerleri, spesifik ısı emme katsayıları ile benzer davranışlar göstermiştir.

Anahtar Kelimeler: Manyetik malzemeler, nanoyapılar, kimyasal sentez, manyetik özellikler.

1. INTRODUCTION

The origins of magnetic behavior in ferrites lie in the interactions of two different sublattices. For the last few decades, the enhancement of the ability to miniaturize ferrites to nano size enables their primary use in biotechnology. Nanosized ferrites' controllable magnetic anisotropy strength, sufficiently high magnetic moments, chemical stability, and low toxicity and other properties which make them suitable for specific technological and biomedical applications [1-5]. Understanding and controlling the magnetic behavior of ferrites can increase their potential use in information storage, sensors, catalyst, water decontamination, adsorbents, enzyme supports, targeted drug delivery, tissue engineering, local hyperthermia, ferrofluids and contrast agents in nuclear magnetic resonance imaging. Furthermore, nowadays, iron based oxides have found increasing interest in biomedical applications such as

magnetic resonance imaging (MRI), hyperthermia, cellular therapy, tissue repair, drug delivery, magnetoception, biological nanosensors due to their unique characteristics [6-12]. Biomedical applications of ferrite nanoparticles in magneto-hyperthermia are widely investigated due to their ability to increase the temperature of body tissue to eradicate cancer cells by heating. In general, for successful application, the size of ferrite particles should decrease to single domain size and then the particles are monodispersed in a magnetic fluid that allows a controllable ejection on the cancer tumors [13]. Monodisperse nanoparticles cause an equal amount of heating over the tumor region under the applied AC magnetic field [13, 14].

The magneto-heating process is mainly affected by superparamagnetic sized and monodispersed magnetic particles due to the reasons as follows:

1. The mechanism of magneto-heating becomes dependent on Neel relaxation instead of Brownian relaxation below the single domain size region [15]. In that case, the magnetic anisotropy value determines the effectiveness of each relaxation type. While the Neel relaxation is effective above a threshold value (in the superparamagnetic state), an increase in anisotropy causes the Brownian relaxation to become dominant so that the heat originating through the Brownian rotation can thus improve the SAR (Specific Heat Absorption Ratio) value [16].

2. A controllable temperature increase can be only managed by homogeny and narrow size distribution [17]. Furthermore, the controllable intended magneto-heating with narrow size distribution lets us use a few magnetic particles so that we decrease the possibility of toxicity for the organism [2, 18, 19].

3. The decrease of particle size also causes a decrease in Curie temperature (Tc) close to the room temperature; thus, the low Tc value also protects the organism from overheating. Above the Tc, the particles display paramagnetic behavior and the AC magnetic field cannot cause an increase in the temperature in the paramagnetic state. This restriction protects the healthy tissues from the damage of high temperatures [19-22].

The properties of low toxicity, suitable magnetization, and simple fabrication make the ferrite particles particularly appropriate for hyperthermia treatment [23]. However, studies show that surface modifications cause insufficient bio-coherence [24]. Thus, magnetic nanoparticles were coated by bio-coherent materials such as Au and Pt; however, the increase in temperature observed was lower than expected because these metals also act as a magnetic shield [22]. Polymers are also used as a biocompatible material on magnetic nanoparticles in hyperthermia applications; however, the temperature increase can remove polymers from the ferrite surface, resulting in toxicity. [25].

Similarly, highly toxic nature of magnetic nanoparticles, deriving from the surface reactivity of magnetic nanoparticles, also constrains their use in biological applications [26]. As a preventive, magnetic nanoparticles are coated with a nonmagnetic shell, thus declining surface reactivity, in order to adapt to vivo applications [27, 28]. SiO_2 is the one such widely used coating material due to its stability to many chemicals [28, 29] and temperature variations [30]. In addition, SiO_2 can perform neither nor oxidation reactions with the core material [31]. As a consequence of these attributes, SiO_2 is known as a bio-compatible material in vivo organisms.

In our study, the properties of Ni-Ferrite nanoparticles were analyzed before and after SiO_2 coating. However, coating with SiO_2 should cause a change in the magneto-heating mechanism as well as the effective anisotropy of Ni-ferrite nanoparticles. DC magnetization and AC magnetic susceptibility measurements of the nanoparticles were employed to investigate the microscopic relaxation and hysteresis. Mechanisms (including relevant parameters such as the amplitude of alternating magnetic field, particle size distribution, anisotropy constant, saturation magnetization, surface treatment, the concentrations of particles) responsible for heat

dissipation in the FM (Ferromagnetic) and SPM (Superparamagnetic) nanoparticles. Magneto-thermal experiments were done to investigate the magnetic media dependent specific absorption rate (SAR) in the AC magnetic field.

2. EXPERIMENTAL

The chemical route employed is the technique of synthesizing first developed by Caruntu et. al. [32-34]. The only deviation from Caruntu et. al's methodology was that Ar gas flow was used in our work instead of N_2 for removal of the evaporating or releasing gases from the vial (with a rate of 60 cc/min) and for cooling (with a rate of 20 cc/min), the top of the Schlenk flask. $NiFe_2O_4/SiO_2$ core–shell structure were formed by using Lee et. al's technique [35].

$NiCl_2 \cdot 6H_2O$ (98 %) salt was combined with $FeCl_3 \cdot 6H_2O$ (97 %), DEG (99 %), oleic acid (OA) (95 %), sodium hydroxide (NaOH) (97%) for synthesizing $NiFe_2O_4$ nanoparticles and washed with ethanol (99.5 %), methanol (99 %) and toluene (99.8 %), respectively. Synthesized nanoparticles were precipitated in a centrifuge with a speed of 4000 rpm for 20 min and then washed carefully twice in methanol and ethanol. The precipitation processes were repeated in a toluene solution with an 8000 rpm centrifuge speed. The resulting nanoparticles were then air-dried. According to work by Murai et. al., centrifuging alone is not sufficient to remove the oleic acid from the surface of ferrites [36]. It is emphasized that after centrifuging in a toluene solution for several times, the oleic acid thicknesses around the ferrites are between 1.0 nm and 1.2 nm [36]. Thus, the synthesized $NiFe_2O_4$ nanoparticles are defined as $NiFe_2O_4$ nanoparticles in oleic acid. Finally, the nanoparticles in oleic acid were coated with SiO_2 using the technique of water in oil microemulsion with a base catalysis of tetraethyl orthosilicate (TEOS). During the coating process, Igepal CO-520 was used as a surfactant [35].

The thermal treatment of synthesized particles, in oleic acid and coated with SiO_2, was monitored with differential thermal and thermogravimetric analysis (DT-TGA) employing a TG/DTA6300

model analyzer under oxygen or nitrogen flow at 40 mL/min with α-Al_2O_3 reference container. The heating rate was 10 ºC/min from the temperature of 30 ºC to 800 ºC.

The crystal structures of synthesized particles were analyzed using XRD patterns, recorded in the 2θ range of 10º and 100º using a CoK_α radiation with an EQUINOX 1000 X-ray diffractometer. The particle sizes were determined using a JEOL 2010-F model transmission electron microscopy (TEM) with a field emission gun operated at 200 keV.

Magnetization and AC susceptibility measurements were performed with a Quantum Design Physical Property Measurement System (PPMS) magnetometer. The magnetization versus temperature variations σ(T) was obtained using the standard zero field cooled (ZFC) and field cooled (FC) procedures in the temperature range of 5-300K with an applied field of 500 Oe. The magnetization versus field variations σ(H) measured at 5 K and 300 K temperatures in the field of ± 3 T. The AC susceptibility measurements were carried out in the frequency range of 10 Hz - 10k Hz as a function of temperature in the range of 5 to 300 K operating at AC amplitudes of 10 Oe to obtain AC susceptibility variations σ(T) for the real ($\chi^{'}$) parts.

Magneto-thermal characterization has been performed in a homemade setup using power generator, fiber optic thermometer, and data acquisition system. It was possible to raise the temperature of the sample to 50 ºC by supplying an AC magnetic field of 6.4 kA/m at 303 kHz with the setup. Biological limitations should be taken into consideration when employing the AC field and frequencies, which should be less than the multiplication of the field 18 kA/m and frequency 100 kHz [37-39]. The results of the magneto-thermal measurements were used to calculate Specific Absorption Rate (SAR) values.

3. RESULT AND DISCUSSIONS

The structural analysis of the particles was obtained using the XRD patterns shown in Figure 1a. The peaks are in accordance with the ICDD

cards of $NiFe_2O_4$, having pdf # 00-023-1119. No additional peak is realized. Furthermore, the size distributions of the particles are obtained by the TEM figures. Only the TEM figure (Figure 1b) for $NiFe_2O_4@SiO_2$ nanoparticles synthesized in 1.5 ml TEOS is shown; size distribution is shown in Figure 1c. The size analyses were extended by fitting the size frequencies to the lognormal distribution function (1) as shown in Figure1c.

$$P(D) = \frac{1}{\sigma_D \cdot D_0 \sqrt{2\pi}} \cdot \exp\left[-\frac{1}{2}\left(\frac{\ln(D/D_0)^2}{\sigma_D^2} \right) \right] \quad (1)$$

In this equation D, D_o and σ_D represent particle size, average particle size and standard deviation, respectively. As depicted in Figure 1b, the thickness of SiO_2 over the ferrite nanoparticles is homogeneously distributed through all particles. The average particle size of $NiFe_2O_4$ is 5.6 nm and the SiO_2 layer thickness over the core particles is changed from 0 nm to 14.1 ± 0.1 nm changing the amount of TEOS used in syntheses. The 1.5 mL TEOS enabled ferrites to be covered with SiO_2 in a thickness of 13.6 ± 0.1 nm as seen in Figure 1b.
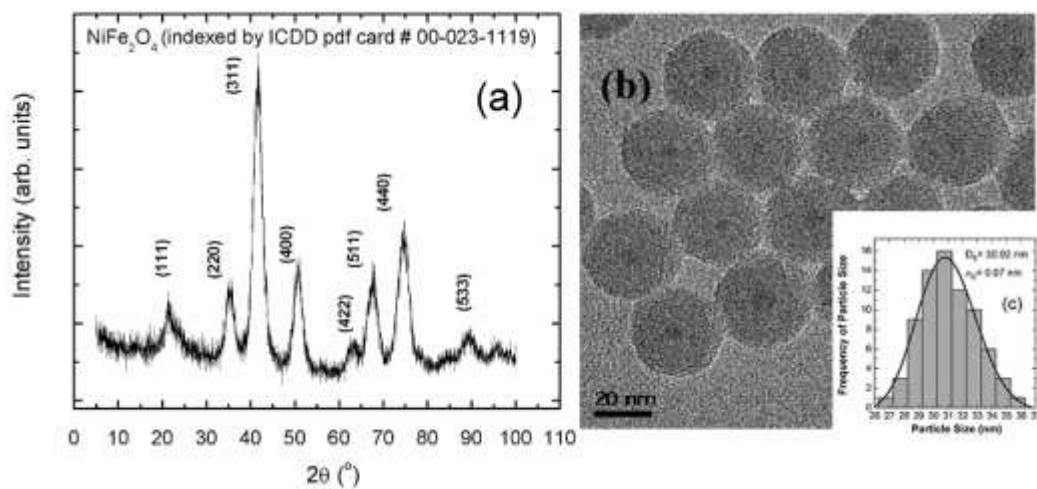
Figure 1. (a) XRD patterns of synthesized $NiFe_2O_4$ nanoparticles and (b) TEM figures of SiO_2 coated $NiFe_2O_4$ (The particle size frequencies are shown in right inset (c)).

The thermal stabilities of oleic acid and SiO_2 coated particles were analyzed using DT-TGA measurements. The DT-TGA measurement of pure oleic acid was taken in order to make a comparison with the SiO_2 coated particles as shown in Figure 2a. DT-TGA results are shown in Figure 2b, 2c, and 2d. for oleic acid and SiO_2 coated samples.
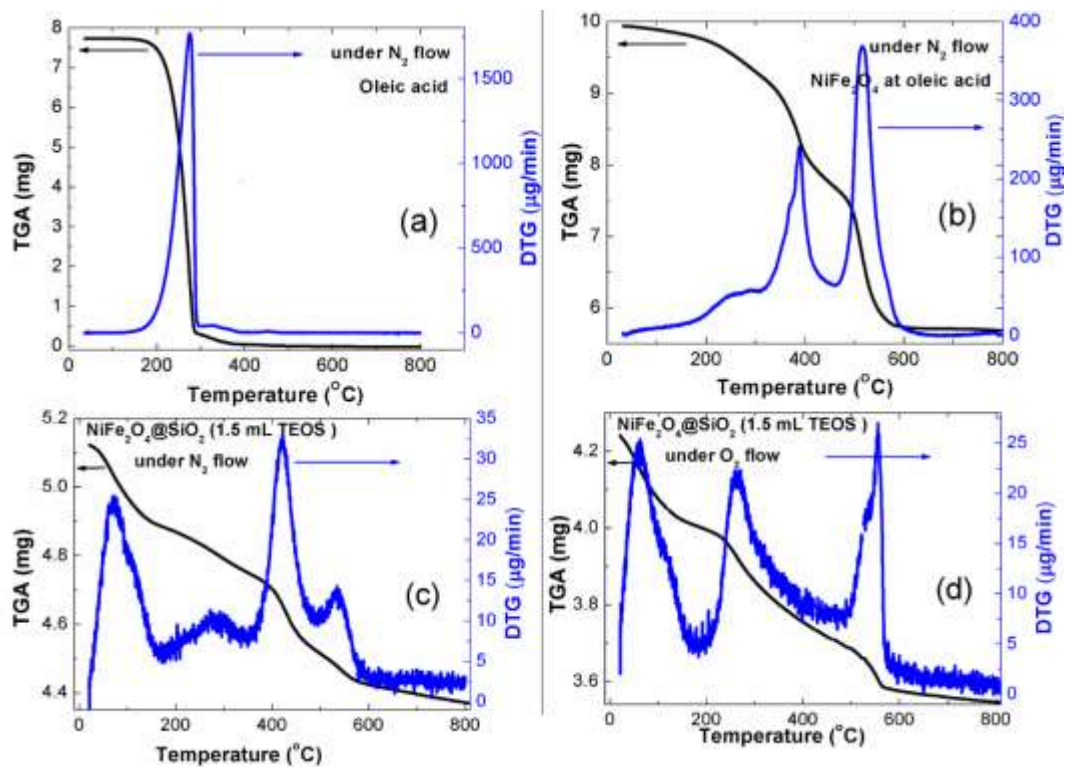
Figure 2. The DT-TGA curves of (a) oleic acid, (b) $NiFe_2O_4$ particles in oleic acid, (c) and (d) $NiFe_2O_4$ @ SiO_2. The figures in between (a)-(c) were taken under N_2 and (d) under O_2 gas flows.

Five different mass losses rates are observed in the TGA spectra taken under N_2 flow for $NiFe_2O_4$ nanoparticles in oleic acid. The first mass loss is observed in the temperature interval of 30 °C and 200 °C at around 3.25 % - 3.50 % due to the evaporation of water, methanol, and ethanol [31]. Because of the evaporation of diethyl glycol (DEG) ($T_{evaporation} \cong 244$ °C), the other mass loss (~1.5 %) is observed between 236 and 250 °C. The mass loss at around 300-500°C (20 % - 22 %) and 290 – 315 °C (4 % - 5 %) originates from loosening the first and seconds of weakly bonded functional groups (COOH) around the nanoparticles, respectively [40-42]. The second order mass loss is also observed at 276 °C as seen in a DT-TGA spectra of pure oleic acid under N_2 (figure 2a) gas flows. Moreover, the first order loss, shown in Figures 2b, originates from the breaking of strongly bonded oleic acids and ferrite nanoparticles as mentioned in various studies [40-42]. The first order loss is

observed at 379.7 °C. The last mass loss is formed between 500 °C and 800 °C. This loss is observed in two steps. The first step, mass loss at around 517°C for $NiFe_2O_4$ nano ferrites, correlates to the phase transitions of iron atoms in the lattice [41-43]. The phase transitions occur in the thermodynamically more stable phases, FeO and α-Fe, and during the transition, oxygen atoms should release [41-43]. The second step, mass loss at around 570°C for $NiFe_2O_4$ nano ferrites, originates from the evaporation CO, CO_2 and H_2O gases from the sample. These gases, after reaching sufficient energy, form unbonding and releasing oxygen atoms from C and H atoms in oleic acid.

The mass loss for SiO_2 coated samples is around 5 % in the temperature range of 30°C - 200°C because of the evaporation of water, methanol ($T_{evaporation}$=64.7°C), and the other chemicals. In addition, the mass losses are observed in temperature ranges of 420°C and 440°C for N_2

flow and in temperature ranges of 265°C - 320°C for O_2 flow. These losses originate from evaporation of oleic acid ($T_{evaporation}$ =360°C) and Igepal CO-520 ($T_{evaporation}$ = 200-300°C), which was used during the SiO_2 coating. The phase transitions of Fe atoms due to a mass loss of around 1.5 – 2 % are observed in the temperature range of 540°C and 550°C under N_2 flow and in the temperature range of 535°C and 550°C under O_2 flow for SiO_2 coated samples. This ratio is lower than it is uncoated $NiFe_2O_4$ nano ferrites. The phase transitions were observed at around 540°C – 550°C as seen in Figure 2.

Magnetization versus field ($\sigma(H)$) curves were obtained at 5 K and 300 K as shown in figure 3. The measured magnetic saturation values, 32.2±0.2 emu/g (300 K) and 41.5±0.2 emu/g (5 K) of $NiFe_2O_4$ particles, are lower than that of the bulk value, 56 emu/g at 300K [44,45]. This anomalous magnetic behavior was correlated with the absence or presence of antiphase domain boundary structural defects. This antiphase boundary structural defects create high angle antiferromagnetic bonds that reduce the magnetization in crystalline magnetite nanoparticles [46]. Moreover, the zero coercivity values at 300 K in s (H) curves, shown in Figure 3a, assign superparamagnetic states, which mean thermal energy became dominant over magnetic energy. In addition, the similar results are also obtained for particles coated with SiO_2. Superparamagnetic behavior at room temperature of coated $NiFe_2O_4$ nanoparticles is plotted at the inset of Figure 3a and Figure 3b. A small impact of the coating by the SiO_2 layer is obtained at cryogenic temperatures. These are a 1 K shift in blocking temperature (T_B) to high temperature from 11.3±0.5 K to 12.3±0.5 K as seen in Figure 3 and an increase in coercivity values from 115 Oe to 122 Oe by SiO_2 coating. The DC measurements, although not giving direct information on the magneto-thermal character, do reveal that the size of particles is in the single domain range, which is suitable for the hysteresis losses to be used in hyperthermia applications. However, the high anisotropy of the particles designates the efficient size ranges for hysteresis losses [47].
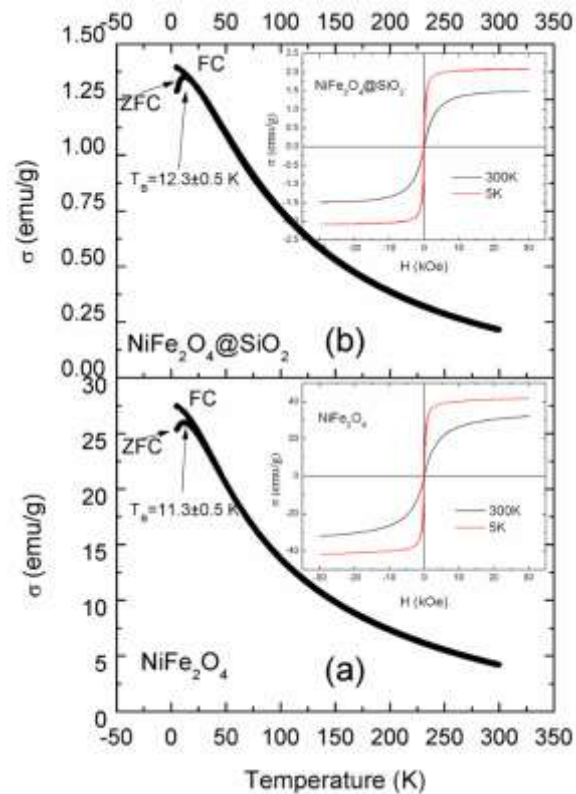
Figure 3. Magnetization versus temperature curves of $NiFe_2O_4@SiO_2$ and $NiFe_2O_4$ nanoparticles taken under 100 Oe. The insets show the magnetization versus magnetic fields at 5 K and 300K.

Thus, the magneto-thermal treatment is highly sensitive to crystal size and magnetic anisotropy change [48]. In addition, the blocking temperature in the cryogenic temperatures assigns Neel relaxations to be effective during the magneto-thermal treatments [49]. Furthermore, the decrease in particle size causes an increase in the magnetic anisotropy of the particles. The increase of anisotropy is one of the main sources of a significant amount of magneto-heat energy. However, the DC magnetization measurements do not give direct information about the magnetic anisotropy of the particles.

The magnetic anisotropies of particles are obtained by AC magnetic susceptibility analyses taken from 10 Hz to 10 kHz frequencies shown in Figure 4. The analyses were done for both $NiFe_2O_4@SiO_2$ and $NiFe_2O_4$ nanoparticles by using Vogel-Fulcher law. The results show that the magnetic nanoparticles as slightly interacting [50]. The

magnetic relaxation in Vogel–Fulcher law occurs within the Néel mechanism and is defined by the equation of (2).

$$T_B \ln\left(\frac{\tau}{\tau_0}\right) = \frac{K_{Eff}V}{k_B} + T_0 \ln\left(\frac{\tau}{\tau_0}\right) \qquad (2)$$

τ, τ_0, k_B, $K_{eff}V$ and T_B are assigned to the relaxation time, the characteristic relaxation time, the Boltzmann constant, the anisotropy energy ($E_a = K_{eff}V$), and blocking temperature, respectively. The AC susceptibility curves are fit to $T_M \ln(\tau/\tau_0)$ versus $\ln(\tau/\tau_0)$ lines and the slope is used to calculate the Vogel-Fulcher temperature (T_0) and anisotropy energies (E_a) [51]. The calculations were done using different relaxation time (τ_0) values, 10^{-9}, 10^{-10}, 10^{-11} and 10^{-12} s, to find the best approximations. The best fit for $NiFe_2O_4$ nanoparticles was obtained for $\tau_0 = 10^{-9}$ s as shown in Figure 4, and the effective magnetic anisotropy calculations are also demonstrated in Table 1.
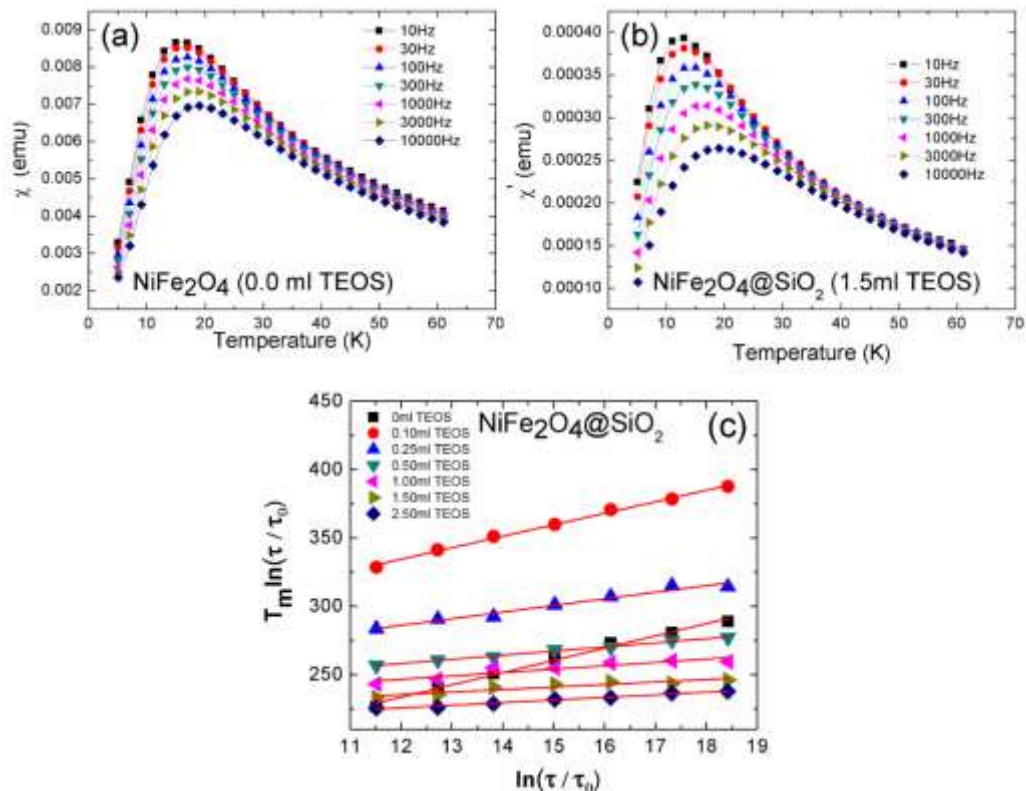
Figure 4. (a) AC susceptibility curves of $NiFe_2O_4$ particles, (b) AC susceptibility curves of $NiFe_2O_4$ @SiO_2 particles and (c) fitting the AC susceptibility curves of $NiFe_2O_4$ @SiO_2 particles to the Vogel-Fulcher law. (Experimental data are shown by the dots and the linear fit shown by the lines). (Reproduced from Ref. [52]).

The Vogel-Fulcher law was also used for SiO_2 coated $NiFe_2O_4$ nanoparticles. The AC susceptibilities and a linear fit to the Vogel-Fulcher law are shown in Figure 4a-4b and Figure 4c, respectively. The values were also calculated for $\tau_0 = 10^{-9}$ s. The T_0 values, which were obtained from the slopes of the $T_M \ln(\tau/\tau_0)$ versus the $\ln(\tau/\tau_0)$ lines, were put on the Table 1. The highest T_0 is observed for the uncoated sample and, the increase of SiO_2 thickness causes a decrease in T_0. The decrease in T_0 assigns the decrease of interparticle interaction with SiO_2. On the other hand, the effective anisotropy (K_{eff}) values were obtained from the intercept point on the $T_M \ln(\tau/\tau_0)$ axis. The results reveal the decrease of anisotropy with the increase of SiO_2 thickness which is attributed to the increase of the distance between the cores ($NiFe_2O_4$) of adjacent particles. The effective magnetic anisotropy values for each particle were also given in Table 1. The results were taken from our previous study for $NiFe_2O_4$ particles [52]. The anisotropy of the nanoparticles increases for the amount of 0.10 ml TEOS used in synthesis. The increase in effective anisotropy is the consequence of removing the oleic acid from the surface, an action that makes the particles closer to one other and that causes a change in effective anisotropy [53]. An exponential decrease follows in the effective anisotropy by further increasing the amount of TEOS.

Table 1. Calculated specific heat absorption ratios, the Vogel-Fulcher temperatures (T_0) and the effective anisotropy values.

Thickness of SiO$_2$ (nm)	Mass of Ni-Ferrite(mg)	Mass of SiO$_2$(mg)	Mass of Hexane(mg)	Mass of Water (mg)	SAR$_{Theo.}$ (W/g)	d(ΔT)/dt$|_{t\to0}$(K/s)	SAR$_{Exp.}$ (W/g)	T$_0$ (K) from Ref. [51]	K$_{effective}$ (kJ/m^3) from Ref. [51]
0.0	4.7	-	654.8	-	1.9	0.0075	2.4±0.2	9.0±0.4	16.4
1.7	4.4	5.5	-	998.2	2.9	0.0039	3.7±0.2	8.4±0.2	30.5
7.9	4.4	15.4	-	998.2	2.8	0.0037	3.5±0.2	5.2±0.4	29.1
9.0	4.4	35.2	-	998.2	2.8	0.0032	3.1±0.2	3.3±0.1	28.5
10.9	3.6	55.8	-	998.2	2.7	0.0028	3.3±0.2	3.2±0.4	26.4
13.6	3.2	66.2	-	998.2	2.7	0.0027	3.6±0.2	2.2±0.3	25.9
14.1	2.3	72.0	-	998.2	2.6	0.0017	3.2±0.2	1.7±0.1	25.7

The analyses via AC susceptibility curves give specific information on effective anisotropies of all particles, $NiFe_2O_4$ in oleic acid and $NiFe_2O_4$@SiO_2. The results prove that ferrite nanoparticles' surface interaction between SiO_2 and the distance between the cores of the particles is the main parameter for effective magnetic anisotropy.

The hyperthermia analyses were done with SAR measurements. The magneto-heat measurements of uncoated $NiFe_2O_4$ and $NiFe_2O_4$@SiO_2 nanoparticles were taken by making nanofluid in 1 ml hexane and in 1 ml water media, respectively. The theoretical (SAR$_{Theo.}$) and experimental (SAR$_{Exp.}$) results were shown in Table 1. The theoretical SAR values were analyzed using the combinations of Brownian and Neel approximations as shown in a previous study [17]. While the hydrodynamic radius leads to an increase in the Brownian relaxation time dependent heat dissipation [54], the Neel relaxation dependent heat dissipation is associated with the changes in the direction of magnetic moments [55]. Therefore, both relaxations produce a magnetic response to an alternating magnetic field [54]. Thus, although our

samples have the effect of Brownian relaxation, the Brownian relaxation cannot be the main source for magneto-heating in this work. Because the particles are in a superparamagnetic state, the magnetic response of Ni-Ferrite nanoparticles obeys the Neel type relaxation. Therefore, intraparticle magnetic moments should be dominant in the magneto heat effect in these particles. The SAR is calculated with the equation 3 [17].

$$SAR = \frac{\sum_i c_i m_i}{m_{mag}} |d(\Delta T)/dt|_{t \to 0} \qquad (3)$$

c_i, m_i, m_{mag} and $\Delta T(t)$ are used to indicate the heat capacity of the ith particle, the mass of the ith particle, the mass of the magnetic particle and temperature increments, respectively. The increment of the temperature is defined by Equation 4.

$$\Delta T = a(1 - e^{-bt}) \qquad (4)$$

where a and b are saturation temperature value(s) and relaxation time(s), respectively.

In the linear region, where $t \to 0$, $|d(\Delta T)/dt|_{t \to 0}$ is equal to a·b.

The SAR$_{Exp.}$ values were calculated by using the ΔT versus time curves as seen in Figure 5.
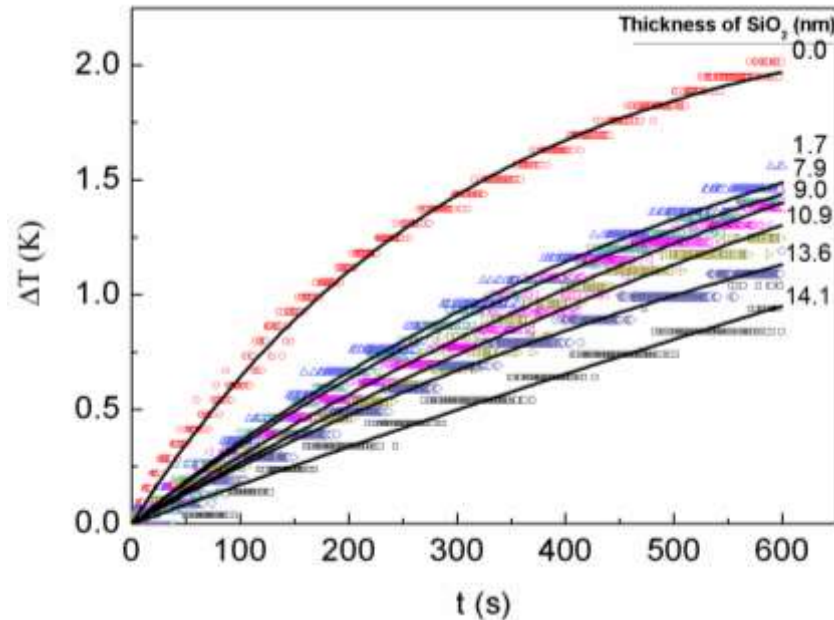
Figure 5. Time versus Magneto-heat measurements and the fits to the magneto-heat measurements for NiFe$_2$O$_4$@SiO$_2$ nanoparticles.

The calculations were done for the heat capacity values 2046 J/(kg K), 703 J/(kg K), 830 J/(kg K), 4181.8 J/(kg K), and 2260 J/(kg K) of oleic acid, SiO$_2$, NiFe$_2$O$_4$, water and hexane, respectively. In addition, specific density and viscosity of water and hexane are taken as 998.2071 kg/m^3 and 1.002 mPs, and as 654.8 kg/m^3 and 0.294 mPs, respectively. The uncoated particles have the lowest effective anisotropy as well as the lowest SAR value. The coatings with SiO$_2$ cause an increase in values, effective anisotropy, and the SAR. The increase of SiO$_2$ thickness causes a specific enhancement in SAR values while the effective anisotropy increases. The result shows that the change at SAR and effective anisotropy values are coherent to each other. In contrary, the SAR values are not correlated with the enhanced interactions of cores of particles. The smallest SAR value was obtained at the minimum distance between the adjacent particles, and coating with SiO$_2$ causes an increase at SAR values, as shown in Table 1.

5.CONCLUSION

In this study, monodisperse $NiFe_2O_4$ ferrite nanoparticles in oleic acid and at SiO_2 matrix were synthesized via a chemical route. The thermal stability of $NiFe_2O_4$ nanoparticles was determined up to 540°C – 550°C by covering ferrites with SiO_2. Furthermore, the ferrites at SiO_2 were isolated from their environments during the phase transitions of ferrites in oleic acid, depending on gas flow atmosphere. The particles behaved superparamagnetic at room temperature. Accordingly, we have found a specific relation between effective anisotropy and SAR values. The results show that the coating with SiO_2 increases the suitability of $NiFe_2O_4$ nanoparticles to the hyperthermia applications by decreasing magnetic interactions with enhanced SiO_2 thicknesses.

REFERENCES

[1]. Tang S.Q., Moon S.J., Park K. H., Paek S. H., Chung K. W., Bae S. Feasibility of TEOS Coated $CoFe_2O_4$ Nanoparticles to a GMR Biosensor Agent for Single Molecular Detection. Journal of nanoscience and nanotechnology, 2011; 11(1): 82-89.

[2]. Pradhan P., Giri J., Samanta G., Sarma,H. D., Mishra K.P., Bellare J., ... & Bahadur D., Comparative evaluation of heating ability and biocompatibility of different ferrite-based magnetic fluids for hyperthermia application. Journal of biomedical materials research Part B: Applied Biomaterials, 2007; 81(1): 12-22.

[3]. Teja A.S., Koh P.Y. Synthesis, properties, and applications of magnetic iron oxide nanoparticles. Progress in crystal growth and characterization of materials, 2009; 55(1): 22-45.

[4]. Wu W., He Q., Jiang C. Magnetic iron oxide nanoparticles: synthesis and surface functionalization strategies. Nanoscale Research Letters, 2008; 3(11): 397-415.

[5]. Jia C.J., Sun L.D., Luo F., Han X.D., Heyderman L.J., Yan Z.G., Hayashi N. Large-scale synthesis of single-crystalline iron oxide magnetic nanorings. Journal of the American Chemical Society, 2008; 130(50): 16968-16977.

[6]. Fortin J.P., Wilhelm C., Servais J., Ménager C., Bacri J.C. Gazeau F. Size-sorted anionic iron oxide nanomagnets as colloidal mediators for magnetic hyperthermia. Journal of the American Chemical Society, 2007; 129(9): 2628-2635.

[7]. Rogers W.J., Meyer C.H., Kramer C.M. Technology insight: in vivo cell tracking by use of MRI. Nature Clinical Practice Cardiovascular Medicine, 2006; 3(10): 554-562.

[8]. Gupta A.K., Gupta M. Synthesis and surface engineering of iron oxide nanoparticles for biomedical applications. Biomaterials, 2005; 26(18): 3995-4021.

[9]. Perez J.M., Josephson L., Weissleder R. Use of magnetic nanoparticles as nanosensors to probe for molecular interactions. ChemBioChem, 2004; 5(3): 261-264.

[10]. Jain T.K., Reddy M.K., Morales M.A., Leslie-Pelecky D.L., Labhasetwar V. Biodistribution, clearance, and biocompatibility of iron oxide magnetic nanoparticles in rats. Molecular pharmaceutics, 2008; 5(2): 316-327.

[11]. Lee H., Lee E., Kim D.K., Jang N.K., Jeong Y.Y., Jon S. Antibiofouling polymer-coated superparamagnetic iron oxide nanoparticles as potential magnetic resonance contrast agents for in vivo cancer imaging. Journal of the American Chemical Society, 2006; 128(22): 7383-7389.

[12]. Corot C., Robert P., Idée J.M., Port M. Recent advances in iron oxide nanocrystal technology for medical imaging. Advanced drug delivery reviews, 2006; 58(14): 1471-1504.

[13]. Jordan A., Scholz R., Wust P., Fähling H., Krause J., Wlodarczyk W., Felix R. Effects of magnetic fluid hyperthermia (MFH) on

C3H mammary carcinoma in vivo. International Journal of Hyperthermia, 1997; 13(6): 587-605.

[14]. Laurent S., Dutz S., Häfeli U.O., Mahmoudi M. Magnetic fluid hyperthermia: focus on superparamagnetic iron oxide nanoparticles. Advances in colloid and interface science, 2011; 166(1): 8-23.

[15]. Hergt R., Andra W., d'Ambly C. G., Hilger I., Kaiser W.A., Richter U., Schmidt H.G. Physical limits of hyperthermia using magnetite fine particles. IEEE Transactions on Magnetics, 1998; 34(5): 3745-3754.

[16]. Suto M., Hirota Y., Mamiya H., Fujita A., Kasuya R., Tohji K., Jeyadevan B. Heat dissipation mechanism of magnetite nanoparticles in magnetic fluid hyperthermia. Journal of Magnetism and Magnetic Materials, 2009; 321(10): 1493-1496.

[17]. Rosensweig R. E., Heating magnetic fluid with alternating magnetic field. Journal of magnetism and magnetic materials, 2002; 252: 370-374.

[18]. Xie Y., Liu D., Cai C., Chen X., Zhou Y., Wu L., ... & Liu P., Size-dependent cytotoxicity of Fe_3O_4 nanoparticles induced by biphasic regulation of oxidative stress in different human hepatoma cells. International journal of nanomedicine, 2016; 11: 3557.

[19]. Hergt R., Dutz S., Müller R., & Zeisberger M. Magnetic particle hyperthermia: nanoparticle magnetism and materials development for cancer therapy. Journal of Physics: Condensed Matter, 2006; 18(38): S2919.

[20]. Yanada T., Matsuki H., Takahashi M., Satoh T., Minakawa S., Kikuchi S., & Murakami K. Evaluation of temperature sensitive amorphous metal flakes for self-regulated hyperthermia. IEEE transactions on magnetics, 1991, 27(6), 5390-5392.

[21]. Chen Z. P., Roemer R.B., Cetas T.C. Short communication: Errors in the two-dimensional simulation of ferromagnetic implant hyperthermia. International journal of hyperthermia, 1991; 7(5): 735-739.

[22]. Apostolova I., Wesselinowa J.M. Possible low-TC nanoparticles for use in magnetic hyperthermia treatments. Solid State Communications, 2009; 149(25): 986-990.

[23]. Molday R.S., Mackenzie D. Immunospecific ferromagnetic iron-dextran reagents for the labeling and magnetic separation of cells. Journal of immunological methods, 1982; 52(3): 353-367.

[24]. Maaz K., Karim S., Mumtaz A., Hasanain S. K., Liu J., Duan J.L. Synthesis and magnetic characterization of nickel ferrite nanoparticles prepared by co-precipitation route. Journal of Magnetism and Magnetic Materials, 2009; 321(12): 1838-1842.

[25]. Kim D.H., Nikles D.E., Johnson D.T., Brazel C.S. Heat generation of aqueously dispersed $CoFe_2O_4$ nanoparticles as heating agents for magnetically activated drug delivery and hyperthermia. Journal of Magnetism and Magnetic Materials, 2008; 320(19): 2390-2396.

[26]. Sanvicens N., Marco M.P. Multifunctional nanoparticles–properties and prospects for their use in human medicine. Trends in biotechnology, 2008; 26(8): 425-433.

[27]. Chen J.S., Chen C., Liu J., Xu R., Qiao S.Z., Lou X.W. Ellipsoidal hollow nanostructures assembled from anatase TiO_2 nanosheets as a magnetically separable photocatalyst. Chemical Communications, 2011; 47(9): 2631-2633.

[28]. Vogt C., Toprak M.S., Muhammed M., Laurent S., Bridot J.L., Müller R.N. High quality and tuneable silica shell–magnetic core nanoparticles. Journal of nanoparticle research, 2010; 12(4): 1137-1147.

[29]. Yi D. K., Lee S. S., Papaefthymiou G.C., Ying J.Y., Nanoparticle architectures templated by SiO_2/Fe_2O_3 nanocomposites. Chemistry of Materials, 2006; 18(3): 614-619.

[30]. Tang D., Yuan R., Chai Y., An H. Magnetic-Core/Porous-Shell $CoFe_2O_4/SiO_2$ Composite Nanoparticles as Immobilized Affinity Supports for Clinical Immunoassays. Advanced Functional Materials, 2007; 17(6): 976-982.

[31]. Yang H.T., Hasegawa D., Takahashi M., Ogawa T. Achieving a noninteracting magnetic nanoparticle system through direct control of interparticle spacing. Applied Physics Letters, 2009; 94(1): 013103.

[32]. Caruntu D., Remond Y., Chou N. H., Jun M. J., Caruntu G., He J., ... & Kolesnichenko V., Reactivity of 3d transition metal cations in diethylene glycol solutions. Synthesis of transition metal ferrites with the structure of discrete nanoparticles complexed with long-chain carboxylate anions. Inorganic chemistry, 2002; 41(23): 6137-6146.

[33]. Caruntu D., Caruntu G., Chen Y., O'Connor C.J., Goloverda G., Kolesnichenko V.L. Synthesis of variable-sized nanocrystals of Fe_3O_4 with high surface reactivity. Chemistry of materials, 2004; 16(25): 5527-5534.

[34]. Caruntu D., Caruntu G., & O'Connor C. J., Magnetic properties of variable-sized Fe_3O_4 nanoparticles synthesized from non-aqueous homogeneous solutions of polyols. Journal of Physics D: Applied Physics, 2007; 40(19): 5801.

[35]. Lee D.C., Mikulec F.V., Pelaez J.M., Koo B., Korgel B.A. Synthesis and magnetic properties of silica-coated FePt nanocrystals. The Journal of Physical Chemistry B, 2006; 110(23): 11160-11166.

[36]. Murai K., Watanabe Y., Saito Y., Nakayama T., Suematsu H., Jiang W., ... & Niihara K., Preparation of copper nanoparticles with an organic coating by a pulsed wire discharge method. Journal of Ceramic Processing Research, 2007; 8(2): 114.

[37]. Gneveckow U., Jordan A., Scholz R., Brüß V., Waldöfner N., Ricke J., ... & Wust P., Description and characterization of the novel hyperthermia and thermoablation system MFH® 300F for clinical magnetic fluid hyperthermia. Medical physics, 2004; 31(6): 1444-1451.

[38]. Hergt R., Dutz S. Magnetic particle hyperthermia-biophysical limitations of a visionary tumour therapy. Journal of Magnetism and Magnetic Materials, 2007; 311(1): 187-192.

[39]. Jordan A., Wust P., Fählin H., John W., Hinz A., Felix R. Inductive heating of ferrimagnetic particles and magnetic fluids: physical evaluation of their potential for hyperthermia. International Journal of Hyperthermia, 1993; 9(1): 51-68.

[40]. Binder W.H., Weinstabl H.C. Surface-modified superparamagnetic iron-oxide nanoparticles. Monatshefte für Chemie-Chemical Monthly, 2007; 138(4): 315-320.

[41]. Ayyappan S., Gnanaprakash G., Panneerselvam G., Antony M.P., Philip J. Effect of surfactant monolayer on reduction of Fe_3O_4 nanoparticles under vacuum. The Journal of Physical Chemistry C, 2008; 112(47): 18376-18383.

[42]. Zhao S.Y., Lee D.G., Kim C.W., Cha H.G., Kim Y.H., Kang Y.S. Synthesis of magnetic nanoparticles of Fe_3O_4 and $CoFe_2O_4$ and their surface modification by surfactant adsorption. Bulletin of the Korean Chemical Society, 2006; 27(2): 237-242.

[43]. Bodsworth C. The extraction and refining of metals (Vol. 2). CRC Press, 1994.

[44]. Lévy M., Wilhelm C., Siaugue J.M., Horner O., Bacri J.C., Gazeau F.,Magnetically induced hyperthermia: size-dependent heating power of γ-Fe_2O_3 nanoparticles. Journal of Physics: Condensed Matter, 2008; 20(20): 204133.

[45]. Nedelkoski Z., Kepaptsoglou D., Lari L., Wen T., Booth, R.A., Oberdick, S.D.,..& Lazarov V.K. Origin of reduced magnetization and domain formation in small magnetite nanoparticles. Scientific Reports, 2017; 7:, 45997

[46]. Martinez-Boubeta C., Simeonidis K., Makridis, A., Angelakeris, M., Iglesias, O., Guardia P., & Saghi Z., Learning from Nature to Improve the Heat Generation of Iron-Oxide Nanoparticles for Magnetic Hyperthermia Applications. Scientific Reports, 2013; 3: 1652.

[47]. Botez C.E., Bhuiya, A.W., Tackett R.J. Dynamic-susceptibility studies of the interplay between the Néel and Brown magnetic relaxation mechanisms. Applied

Physics A: Materials Science & Processing, 2011; 104(1): 177-181.

[48]. López J.L., Pfannes H.D., Paniago R., Sinnecker J.P., Novak M.A. Investigation of the static and dynamic magnetic properties of $CoFe_2O_4$ nanoparticles. Journal of Magnetism and Magnetic Materials, 2008; 320(14): e327-e330.

[49]. Coşkun M., Korkmaz M., Fırat T., Jaffari, G., H., Shah, S.I. Synthesis of SiO_2 coated $NiFe_2O_4$ nanoparticles and the effect of SiO_2 shell thickness on the magnetic properties. Journal of Applied Physics, 2010; 107(9): 09B523.

[50]. De la Presa P., Multigner M., Morales M. P., Rueda T., Fernandez-Pinel E., & Hernando A., Synthesis and characterization of FePt/Au core-shell nanoparticles. Journal of Magnetism and Magnetic Materials, 2007; 316(2): e753-e755.

[51]. Sánchez J.H., Rinaldi C. Rotational Brownian dynamics simulations of non-interacting magnetized ellipsoidal particles in dc and ac magnetic fields. Journal of Magnetism and Magnetic Materials, 2009; 321(19): 2985-2991.

[52]. Kumar C.S., Mohammad F. Magnetic nanomaterials for hyperthermia-based therapy and controlled drug delivery. Advanced drug delivery reviews, 2011, 63(9), 789-808.